PCCP

RSC Publishing

PAPER

View Article Online
View Journal | View Issue

First-principles study of O_2 activation on ligand-protected Au_{32} clusters

Cite this: *Phys. Chem. Chem. Phys.*, 2013, **15**, 9742

Shengping Yu,[a] Qun Zeng,[b] Zhaoyang Lou,[b] Mingli Yang*[b] and Deyin Wu[c]

Received 25th January 2013,
Accepted 16th April 2013

DOI: 10.1039/c3cp50354b

www.rsc.org/pccp

Poly(*N*-vinyl-2-pyrrolidone) (PVP) is often used to protect active Au clusters from coalescence. The influences of PVP on the O_2 adsorption on Au_{32} clusters were investigated using density functional theory calculations. Various low-lying structures of O_2:Au_{32} and O_2:Au_{32}:PVP complexes, in which the Au_{32} is either neutral or anionic and the O_2 is either molecular or dissociative, were identified. The PVP influences were evaluated in terms of the changes in geometry, adsorption energy, charge redistribution, spin density, and density of states upon PVP pre-adsorption. Our calculations reveal that PVP weakly adsorbs on the cluster surface, with rather small changes in the structural, geometrical and electronic properties that are relevant to the O_2 activation. The activity of neutral or anionic Au_{32} towards O_2 is kept or slightly enhanced by PVP because of the cooperative adsorption of PVP and O_2. This is the structural basis of choosing PVP as the protective ligand for Au clusters.

1. Introduction

Gold is inert in bulk, but manifests extraordinary activity at the nanoscale toward a number of molecules like carbon monoxide,[1–8] molecular oxygen,[9–20] alcohol,[21–24] alkene,[25] *etc.* Recent studies[9–25] revealed that small gold clusters, free or supported, can be effective catalysts in chemical synthesis. Stemming from their high reactivity, bare small clusters, however, have a tendency to assemble with each other and form larger clusters. Since the reactivity of gold clusters is size-dependent, one has to control their size distribution by inhibiting their continuing growth or coalescence in preparation. Capping the small clusters with organic ligands has proven to be an effective way to prevent the clusters from coalescence. Several requirements are applied to these ligands. In addition to appropriate binding and coverage onto cluster surfaces, the ligands should not lower the cluster reactivity significantly. The commonly used ligands for Au cluster protection include phosphine,[26] thiolate,[27] selenolate,[28] poly(*N*-vinyl-2-pyrrolidone) (PVP),[29] alkyne,[30] *etc.*, among which PVP stabilized Au clusters are promising for catalytic applications.[31–33] Tsunoyama *et al.*[31] found that Au_n:PVP clusters oxidize p-hydroxybenzyl alcohol selectively into the corresponding aldehyde without degradation. Moreover, Au_n:PVP clusters exhibit high activity for aerobic oxidation of alcohol.[32,33]

Although the interaction of bare Au clusters with adsorbates has been extensively investigated in many theoretical studies,[1–20] the structures of ligand-protected Au clusters, in particular their reactivity, have not yet been well addressed. Garzón *et al.*[34] found in a density functional theory study that the structure of a thiol-protected Au_{38} cluster, $Au_{38}(SR)_{24}$, consists of a symmetric Au core and surrounding $[AuSR]_4$ units. Häkkinen *et al.*[35] proposed a ''divide-and-protect'' concept to understand the structures of thiolate-protected Au nanoparticles based on DFT calculations. In this concept, the Au atoms exhibit different electron configurations, either in the Au(0) or in the Au(I) state. The structures of $Au_{12}(SR)_9^+$,[36] $Au_{25}(SR)_{18}^+$,[37] $Au_{25}(SMT)_{18}^-$,[38] $Au_{25}(SCH_2CH_2Ph)_{18}^-$,[39] $Au_{38}(MT)_x$ (x = 6–24),[40,41] Au_{102}-(p-MBA),[42–44] $Au_{144}(SMT)$,[45] *etc.*, have been investigated by several authors at the DFT level. All of these computations revealed that the ligands affect not only the structures of the capped Au clusters but also their electronic properties, such as their reactivity towards adsorbates.

Many studies[9–20] have focused on the activation of O_2 on bare Au clusters, suggesting that electron transfer from Au_n into the empty antibonding orbital of O_2 generates superoxo- or peroxo-like species that play an important role in boosting the oxidation reactions on Au_n surfaces. However, few studies have been devoted to the O_2 activation on ligand-protected Au_n clusters, which is of great significance in practice. Little is known about the ligand–Au_n interaction, for example, the charge transfer between them, and its effect on the electron-donating/withdrawing ability

[a] *College of Chemistry and Environment Protection Engineering, Southwest University for Nationalities, Chengdu 610041, China*
[b] *Institute of Atomic and Molecular Physics, Sichuan University, Chengdu 610065, China. E-mail: myang@scu.edu.cn*
[c] *State Key Laboratory of Physical Chemistry of Solid Surfaces, Xiamen University, Xiamen 361005, China*

of Au cores, and as a consequence on the O_2 activation. In this study, we performed DFT calculations on the O_2 activation on PVP-pre-adsorbed Au_{32} clusters. Two typical Au_{32} structures, symmetric (I_h) fullerene-like and asymmetric (C_1) compact, were selected. The I_h structure has special stability, known as spherical aromaticity,[46] while the C_1 structure was found to be more stable than the I_h one in later computations.[47] By comparing a number of structural configurations of O_2 on Au_{32}:PVP clusters with those on bare Au_{32} clusters, we analyzed the influence of PVP on the O_2 activation. Since Au_n anions exhibit stronger reactivity towards O_2, both the neutral and anionic states of Au_{32}:PVP clusters were studied. In this article, after outlining the computational strategy in Section 2, we present the computed results in Section 3 for the structures of Au_{32}:PVP, O_2:Au_{32}, and O_2:Au_{32}:PVP in neutral and anionic forms, together with a discussion on the influences of PVP. A summary is given in Section 4.

2. Computational methods

The initial structures of fullerene-like (I_h) and compact (C_1) were taken from earlier studies[46,47] and re-optimized at the DFT level with the Tao–Perdew–Staroverov–Scuseria (TPSS) exchange–correlation functional, which has been recommended for Au-containing systems.[48] Weigend's basis set def2-QZVPP[49] was employed for Au. The effective core potential with relativistic correction of Wood–Boring (MWB)[50] was employed to describe the 60 core electrons, while the valence 5s, 5p, 5d and 6s electrons were described using a triple split-valence basis set plus an augmented polarization function. 2-Pyrrolidone (C_4H_7ON) is used to represent PVP molecules by replacing the large alkyl group with H. It is a reasonable simplification that the alkyl group has large volume favoring to cover the Au_n surface, but its influence on the electronic properties of the pyrrolidone functional group is limited. The def2-QZVPP basis set is also used for C, N, O, and H atoms. All calculations were carried out using the Turbomole suite.[51] To validate our computational strategy, test calculations were performed for the Au dimer and O_2. The computed Au–Au distance for Au_2 is 2.507 Å, in agreement with the measurement of 2.47 Å.[52] The O–O bond length of O_2 is 1.219 Å, in good agreement with early theoretical (1.224 Å[53]) and experimental (1.207 Å[52]) studies.

To locate the optimal interacting patterns of PVP towards Au_{32}, a large number of initial structures were designed by placing PVP at different sites on the Au_{32} surface. All these candidates were screened at the DFT level in order to find the energetically favorable Au_{32}:PVP complexes. Next, based on the low-lying Au_{32}:PVP structures, a number of initial O_2:Au_{32}:PVP structures were constructed by placing O_2 at the independent sites of the Au_{32} surface. A DFT screening was again performed to locate the low-lying O_2:Au_{32}:PVP complexes. For comparison, the interaction of O_2 with bare Au_{32} clusters was also studied in the similar way. As Au_{32} anions are often used in practice, the above procedures were applied to anionic Au_{32} and Au_{32}:PVP systems by simply adding one electron into the systems. Both the molecular and dissociative adsorptions of O_2 were considered in the calculations. Both singlet and triplet states for the neutral systems, and both doublet and quartet states for the anionic systems were examined for all the low-lying isomer structures.

In the self-consistent-field (SCF) calculations, the density tolerance was set to 10^{-6} au. The convergence criteria were set to 10^{-4} au for the gradient and 10^{-6} au for energy in the geometry optimization. The resolution-of-the-identity (RI) approximation[54] and the multipole accelerated RI (MARI) approach[55] were used to speed up the calculations. Spin-polarized calculations were carried out for all the open-shell systems. Harmonic vibrational frequency calculations were performed for the best stable complexes to ensure the obtained structures are true minima on the potential energy surfaces. Two more XC functionals, PBE[56] and BLYP[57,58], were employed in the geometry optimization for some structures. As shown below, these two functionals produce essentially similar results with TPSS[59] for the studied complexes.

3. Results and discussion

3.1 PVP on Au_{32}

The optimized Au_{32} bare clusters, I_h and C_1, retain the same architecture as in previous studies.[46,47] The I_h structure is 0.454 eV more stable than C_1 in neutral form, but its anion is 0.378 eV less stable than the C_1 anion. The I_h structure has three independent adsorbing sites on the surface: apex, edge, and face, while in the asymmetric C_1 structure much more possible adsorbing sites exist, all of which were taken into account in the construction of initial adsorbate–Au_{32} structures.

In all cases, O in PVP is the most active atom towards Au_{32}. Fig. 1 shows the structures of low-lying neutral PVP:Au_{32} complexes in which the O atom binds to one Au atom on the Au_{32} surface. For the I_h structure, apexes are preferred by PVP. Only two apex-adsorbed isomers, which are much more stable in energy than the others, are presented. To distinguish the isomers, we named the isomers as D(T)-I_h(C_1)-a(b, c, ...) hereafter. "D" stands for two subsystems, for example, PVP and Au_{32}, in the system, while "T" for systems with three subsystems. The isomers are ordered as a, b, ..., by their adsorption energy. The apically adsorbed structure D-I_h-a is 0.25 eV more stable than D-I_h-b, as shown in Table 1. Accordingly, D-I_h-a has a shorter Au–O distance (Fig. 1) and a greater amount of transferred charge (Table 1) between the two parts than D-I_h-b. The atomic net charges were evaluated using natural bond orbital (NBO) analysis.[60]

For Au_{32}(C_1), a number of PVP:Au_{32} complexes possess close energy. Only the best four are presented in Fig. 1. Similar to the I_h structure, apexes are the preferred sites for PVP adsorption. The interaction energies of the best four PVP:Au_{32}(C_1) are much higher than those of PVP:Au_{32}(I_h) complexes, indicating that Au_{32}(C_1) has a greater tendency to adsorb PVP than Au_{32}(I_h) does. The O–Au distances of PVP:Au_{32}(C_1) are about 0.11–0.29 Å shorter than those in PVP:Au_{32}(I_h). In both PVP:Au_{32}(C_1) and PVP:Au_{32}(I_h), Au_{32} serves as an electron acceptor. The transferred charge is about 0.05–0.07 e in PVP:Au_{32}(I_h) and 0.09–0.22 e in PVP:Au_{32}(C_1). The spherical aromaticity of Au_{32}(I_h)[46] resists any charge transfer against its 32-electron stability, resulting in a weaker interaction in PVP:Au_{32}(I_h) than in PVP:Au_{32}(C_1).

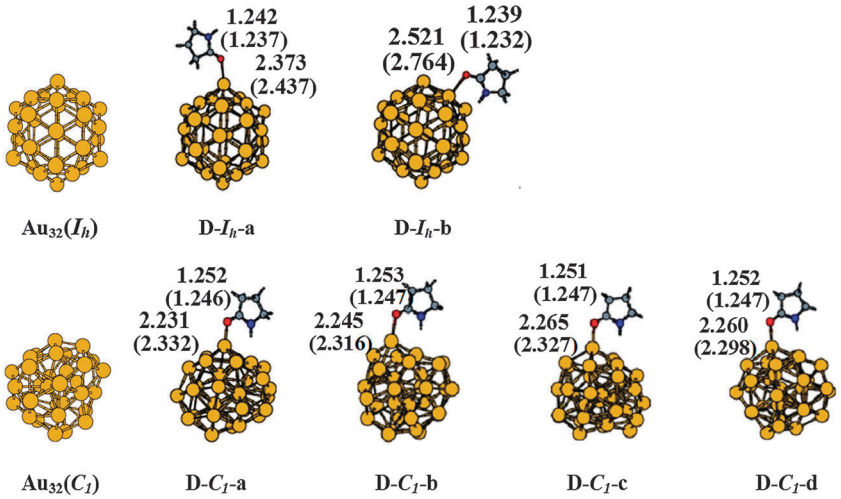

Fig. 1 TPSS/def2-QZVPP optimized structures of neutral and anionic $Au_{32}(I_h)$, $Au_{32}(I_h)$:PVP, $Au_{32}(C_1)$ and $Au_{32}(C_1)$:PVP. All bond lengths are in Å. In parentheses are bond lengths of anionic complexes.

Table 1 Adsorption energy (E_{ads}, in eV), net charge (in au) and spin density (in au) of neutral and anionic $Au_{32}(I_h)$:PVP and $Au_{32}(C_1)$:PVP complexes

		Net charge		Spin density	
	E_{ads}	PVP	Au_{32}	PVP	Au_{32}
D-I_h-a	0.35	0.07	−0.07		
D-I_h-b	0.10	0.05	−0.05		
D-C_1-a	0.69	0.11	−0.11		
D-C_1-b	0.69	0.11	−0.11		
D-C_1-c	0.66	0.10	−0.10		
D-C_1-d	0.64	0.09	−0.09		
DA-I_h-a	0.28	0.03	−1.03	0.01	0.99
DA-I_h-b	0.10	0.04	−1.04	0.00	1.00
DA-C_1-a	0.48	0.05	−1.05	0.05	1.05
DA-C_1-b	0.47	0.06	−1.06	0.01	0.99
DA-C_1-c	0.47	0.06	−1.06	0.02	0.98
DA-C_1-d	0.46	0.06	−1.06	0.03	0.97

Similar adsorption patterns were found in the anionic PVP:Au_{32} clusters, but with smaller amounts of adsorption energy and transferred charge, and longer Au–O distances, as shown in Fig. 1 and Table 1. The spin density is localized on the Au_{32} part for all cases. The extra negative charge reduces the electron-withdrawing ability of Au_{32}, resulting in a weaker interaction in the anionic PVP:Au_{32} clusters than in the neutral clusters.

3.2 O_2 on neutral PVP:Au_{32}

The adsorption of O_2 on bare Au_{32} clusters has been studied by Wang and Gong[13] who found that O_2 is dissociatively adsorbed on the I_h or C_1 Au_{32}. We investigated here the adsorption of O_2 on the neutral Au_{32} in the presence of a PVP ligand and compared it with those on bare Au_{32} clusters.

Two kinds of adsorptions, molecular and dissociative, of O_2 were studied for each adsorption pattern, and both the singlet and triplet states were examined for all the structures. We found that the dissociative configurations have lower energy (by about 0.5 eV) than the corresponding molecularly adsorbed configurations for PVP:$Au_{32}(C_1)$, while both the molecular and dissociative configurations have comparative energy for PVP:$Au_{32}(I_h)$.

We first considered the cases of molecular adsorption. The triplet state of low-lying PVP:Au_{32}:O_2 structures was found to be more stable than the corresponding singlet state for all the molecular adsorption configurations. The best four PVP:Au_{32}:O_2 structures, based on the Au_{32} clusters, are displayed in Fig. 2. The electronic properties of all the isomers are presented in Tables 2 and 3. Three functionals, TPSS, PBE, and BLYP, produce similar energy orders for these isomers. The adsorption energies are very low, less than 0.13 eV and 0.18 eV for PVP:$Au_{32}(I_h)$ and PVP:$Au_{32}(C_1)$, respectively, so are the energy splittings among the low-lying isomers. The inclusion of basis set superposition error (BSSE) correction does not change the relative stability of the isomers. The O_2 adsorbs onto the Au_{32} surface *via* an end-on superoxo form. In PVP:$Au_{32}(I_h)$:O_2, the O–O bonds are about 1.22 Å and the Au–O distances vary in a wide range, 2.8–3.6 Å. Only negligible charge transfer occurs between O_2 and the cluster, leaving almost all the spin density at O_2. In PVP:$Au_{32}(C_1)$:O_2, the O–O bonds are slightly lengthened to 1.24 Å and the Au–O distances are between 2.3–2.4 Å. The transferred charge from the cluster to O_2 is as great as 0.18 *e*, while the spin density is mostly localized at O_2 (about 85%), and marginally at Au_{32}. Our calculations reveal that weak interaction between O_2 and PVP:Au_{32} exists for molecular adsorption, and the interaction is slightly stronger in PVP:$Au_{32}(C_1)$:O_2 than in $Au_{32}(I_h)$:PVP:O_2. Compared with the structures of Au_{32}:O_2 corresponding to the best structures of PVP:Au_{32}:O_2, which are shown in Fig. 3, the pre-adsorption of PVP leads to a small increase of 0.10–0.15 eV in the E_{ads} of O_2, and very small changes in the O–O bonds, O–Au distances, net charge and spin density distribution on O_2 (see Fig. 2 and 3, Tables 2 and 3).

In the dissociative adsorption patterns, the O–O bonds are broken by one or more active Au atoms on the surface. The low-lying structures of PVP:O–Au_{32}–O are presented in Fig. 4. The singlet state is more stable than the corresponding triplet state

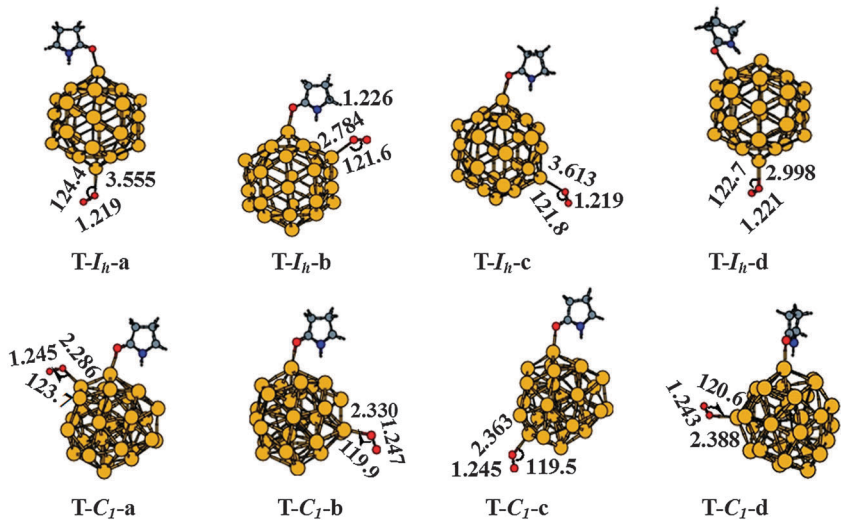

Fig. 2 TPSS/def2-QZVPP optimized structures of neutral $Au_{32}(I_h)$:PVP:O_2 and $Au_{32}(C_1)$:PVP:O_2 in which O_2 is molecularly or dissociatively adsorbed. All bond lengths are in Å. All bond angles are in degree.

Table 2 Relative energy (ΔE, in eV) and adsorption energy (E_{ads}, in eV) of neutral $Au_{32}(I_h)$:PVP:O_2 and $Au_{32}(C_1)$:PVP:O_2 complexes. In parentheses are quantities for corresponding Au_{32}:O_2 complexes without PVP

	TPSS		PBE	BLYP
	ΔE	E_{ads}	ΔE	ΔE
T-I_h-a	0.00	0.13 (0.03)	0.00	0.00
T-I_h-b	0.00	0.13	0.02	−0.01
T-I_h-c	0.01	0.12	0.00	0.01
T-I_h-d	0.30	0.09	0.21	0.26
T-C_1-a	0.00	0.18 (0.02)	0.00	0.00
T-C_1-b	0.01	0.17	−0.01	0.01
T-C_1-c	0.03	0.16	0.01	0.03
T-C_1-d	0.05	0.14	0.03	0.05

Table 3 Net charge (in au) and spin density (in au) of neutral $Au_{32}(I_h)$:PVP:O_2 and $Au_{32}(C_1)$:PVP:O_2 complexes. In parentheses are quantities for corresponding Au_{32}:O_2 complexes without PVP

	Net charge			Spin density		
	PVP	Au_{32}	O_2	PVP	Au_{32}	O_2
T-I_h-a	0.08	−0.07 (−0.01)	0.00 (0.01)	0.00	0.02 (0.02)	1.98 (1.98)
T-I_h-b	0.08	−0.04	−0.04	0.00	0.08	1.91
T-I_h-c	0.07	−0.08	0.00	0.00	0.02	1.98
T-I_h-d	0.05	−0.04	−0.01	0.00	0.04	0.96
T-C_1-a	0.10	0.06 (0.08)	−0.16 (−0.08)	0.01	0.32 (0.18)	1.68 (1.82)
T-C_1-b	0.11	0.07	−0.18	0.00	0.30	1.70
T-C_1-c	0.11	0.06	−0.17	0.00	0.28	1.72
T-C_1-d	0.11	0.05	−0.16	0.00	0.27	1.73

for the dissociative adsorption configurations. Again, the three functionals produce similar energy orders and splittings for the isomers, as seen in Table 4. The largest E_{ads} is 0.21 eV for PVP:O–$Au_{32}(I_h)$–O, about 0.08 eV higher than those in molecular adsorption. Large E_{ads} values, about 0.70 eV, are found in PVP:O–$Au_{32}(C_1)$–O for the best three structures, about 0.50 eV higher than those in molecular adsorption. It is clear that the dissociative adsorption of O_2 is energetically more favorable on the C_1-based structures than those on the I_h-based structures. Short O–Au bond lengths, as short as 1.96 Å, are noted in the dissociated configurations in which the two O atoms are separated by one Au atom and form multiple Au–O bonds on the surface. In all cases, PVP retains its conformation on Au_{32} with very small changes in bond length and net charge, as shown in Table 5. Significant charge transfer, 2.08–2.20 *e*, between Au_{32} and O_2 is noted. Compared to the corresponding PVP:Au_{32} structures, the presence of PVP leads to small changes in the E_{ads} of O_2 and the amount of transferred charge between Au_{32} and O_2 (Tables 4 and 5).

For both the molecular and dissociative adsorptions of O_2 on Au_{32}, the pre-adsorbed PVP group basically retains its structure with tiny changes in bond length, bond angle, and net charge. The interaction between Au_{32} and O_2 is slightly affected by PVP which leads to small changes in the amount of charge transfer (<0.08 *e*) from Au_{32} to O_2, and in the E_{ads} values of O_2 (<0.20 eV).

3.3 O_2 on anionic PVP:Au_{32}

The bare Au_{32}^- cluster exhibits different reactivity from the neutral cluster, as shown in Fig. 3. The anionic $Au_{32}(I_h)$ has much larger E_{ads} values than the neutral cluster, while the anionic $Au_{32}(C_1)$ has larger E_{ads} than the neutral cluster for molecular adsorption, but slightly smaller E_{ads} for dissociative adsorption. The anionic $Au_{32}(I_h)$ becomes active towards O_2 because it has a strong tendency to reconstruct its 32-electron spherical aromaticity by losing the extra electron.

The anionic Au_{32} clusters and their adsorbing complexes are open-shell systems for which both doublet and quartet states were examined. The three functionals produce similar results for the anionic systems. The doublet state structures were found to be always more stable than their corresponding quartet ones.

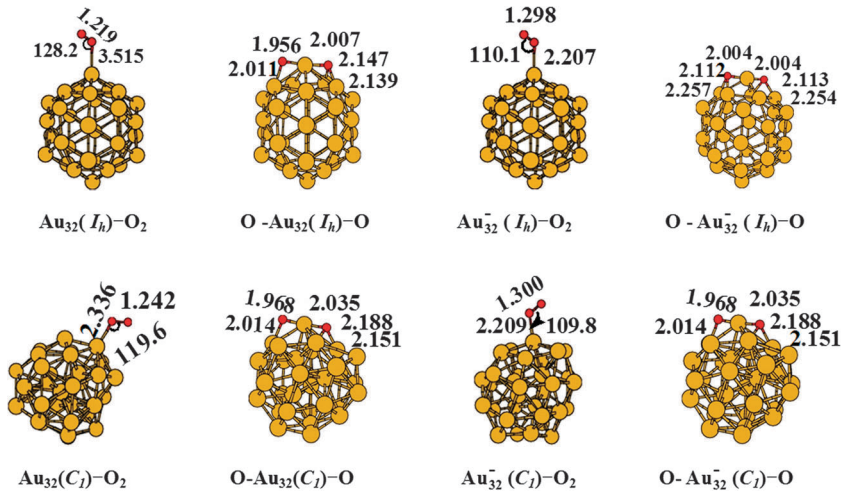

Fig. 3 TPSS/def2-QZVPP optimized structures of Au_{32}:O_2 (triplet) and O–Au_{32}–O (singlet). All bond lengths are in Å.

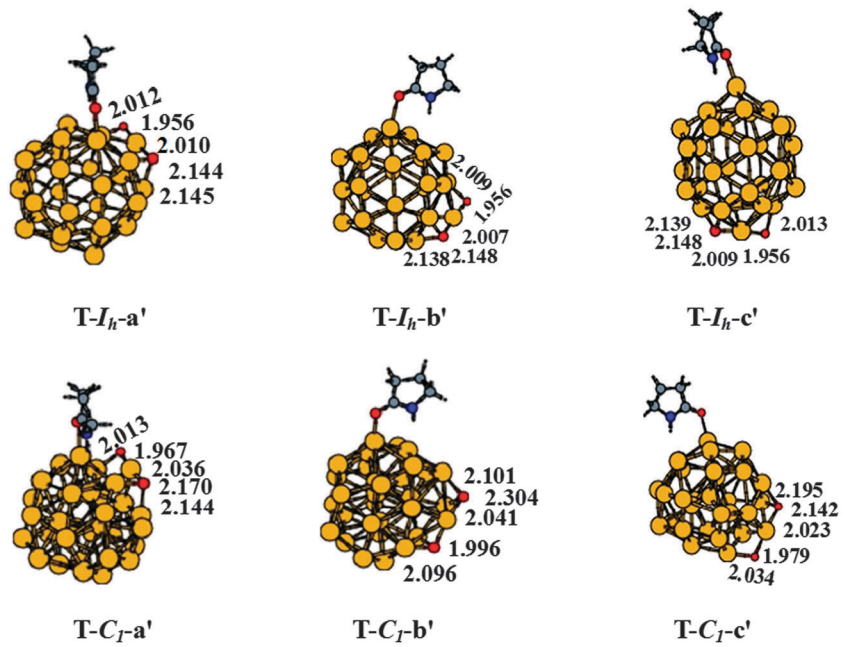

Fig. 4 TPSS/def2-QZVPP optimized structures of neutral O–$Au_{32}(I_h)$–O:PVP and O–$Au_{32}(C_1)$–O:PVP in which O_2 is dissociatively adsorbed. The bond lengths are given in Å.

Only the doublet-state structures are discussed below. Both molecular and dissociative adsorptions of O_2 on the PVP:Au_{32}^- clusters were studied and the dissociative adsorptions have systematically larger E_{ads} values than the molecular adsorptions.

The low-lying structures and electronic properties of molecularly adsorbed O_2 clusters are presented in Fig. 5 and Tables 6 and 7. The O_2 has several adsorption patterns on PVP:Au_{32}^- terminal adsorption in which one O atom of O_2 binds to one Au atom of the cluster, double adsorption in which two O atoms interact with two Au atoms, and bridge adsorption in which one O atom interacts with two Au atoms. The Au–O distances are about 2.21–2.34 Å. The O–O distances are about 1.30–1.32 Å for the PVP:$Au_{32}^-(I_h)$:O_2 and about 1.26–1.27 Å for PVP:$Au_{32}^-(C_1)$:O_2. Correspondingly, the former has larger E_{ads} and a greater amount of transferred charge from Au_{32}^- to O_2 than the latter. The spin density is mostly localized at O_2, about 1.0 au for PVP:$Au_{32}^-(I_h)$:O_2 and about 1.5 au for PVP:$Au_{32}^-(C_1)$:O_2. Our calculations reveal that the O_2 adsorbs more strongly on PVP:$Au_{32}^-(I_h)$ than on PVP:$Au_{32}^-(C_1)$. Compared with the Au_{32}^-:O_2 structures, the pre-adsorption of PVP enhances the interaction of O_2 with $Au_{32}^-(I_h)$, but has a small effect on that with $Au_{32}^-(C_1)$.

The low-lying structures of dissociatively adsorbed O_2 clusters are presented in Fig. 6 and their electronic properties are summarized in Tables 8 and 9. In their anionic form, the I_h- and C_1-based structures do not show distinct differences in their adsorption patterns and E_{ads} values. The Au–O distances are around 2.1 Å. The E_{ads} reaches 1.20 eV for the lowest-energy structures, indicating that the two O atoms form strong bonding with PVP:Au_{32}^-.

Table 4 Relative energy (ΔE, in eV) and adsorption energy (E_{ads}, in eV) of neutral O–Au_{32}(I_h):PVP:O and O–Au_{32}(C_1):PVP:O. In parentheses are quantities for corresponding Au_{32}:O_2 complexes without PVP

	TPSS		PBE	BLYP
	ΔE(eV)	E_{ads}(eV)	ΔE(eV)	ΔE(eV)
T-I_h-a′	0.00	0.21 (0.01)	0.00	0.00
T-I_h-b′	0.05	0.15	0.06	0.06
T-I_h-c′	0.08	0.13	0.07	0.07
T-C_1-a′	0.00	0.73 (0.82)	0.00	0.00
T-C_1-b′	0.02	0.70	0.24	0.12
T-C_1-c′	0.06	0.67	0.22	0.13

Table 5 Net charge (in au) of the neutral O–Au_{32}(I_h)–O:PVP and O–Au_{32}(C_1)–O:PVP in which O_2 is dissociatively adsorbed. In parentheses are quantities for corresponding Au_{32}:O_2 complexes without PVP

	Net charge		
	PVP	Au_{32}	O_2
T-I_h-a′	0.09	2.00 (2.07)	−2.08 (−2.07)
T-I_h-b′	0.08	2.00	−2.08
T-I_h-c′	0.08	2.00	−2.08
T-C_1-a′	0.10	2.04 (2.12)	−2.13 (−2.12)
T-C_1-b′	0.10	2.10	−2.20
T-C_1-c′	0.10	1.98	−2.08

A large amount of negative charge (>2.0 e) moves from Au_{32}^- to O_2. The net charge at Au_{32} changes from negative (about −1.0 e) to positive (about +1.2 e). Most spin density is at Au_{32} and the others at the two O atoms. All the geometrical and electronic quantities reflect that the anionic Au_{32}:PVP forms strong bonding with O_2 in the dissociative adsorption. Compared with the corresponding O–Au_{32}^-–O structures, the presence of PVP leads to an increase in the E_{ads} of O_2 (by about 0.4 eV) and in the charge transfer between Au_{32} and O_2 (by about 0.02 e).

Table 6 Relative energy (ΔE, in eV) and adsorption energy (E_{ads}, in eV) of anionic Au_{32}(I_h):PVP:O_2 and Au_{32}(C_1):PVP:O_2. In parentheses are quantities for corresponding Au_{32}:O_2 complexes without PVP

	TPSS		PBE	BLYP
	ΔE	E_{ads}	ΔE	ΔE
TA-I_h-a	0.00	0.71 (0.42)	0.00	0.00
TA-I_h-b	0.27	0.44	0.26	0.25
TA-I_h-c	0.29	0.42	0.27	0.23
TA-I_h-d	0.29	0.42	0.28	0.25
TA-C_1-a	0.00	0.26 (0.20)	0.00	0.00
TA-C_1-b	0.02	0.24	0.02	0.01
TA-C_1-c	0.07	0.19	0.11	0.09
TA-C_1-d	0.08	0.18	0.00	0.05

Table 7 Net charge (in au) and spin density (in au) of anionic Au_{32}(I_h):PVP:O_2 and Au_{32}(C_1):PVP:O_2. In parentheses are quantities for corresponding Au_{32}:O_2 complexes without PVP

	Net charge			Spin density		
	PVP	Au_{32}	O_2	PVP	Au_{32}	O_2
TA-I_h-a	0.06	−0.41 (−0.49)	−0.65 (−0.51)	0.01	0.04 (−0.17)	0.96 (1.17)
TA-I_h-b	0.05	−0.45	−0.60	0.00	0.03	0.97
TA-I_h-c	0.05	−0.46	−0.59	0.00	0.02	0.98
TA-I_h-d	0.04	−0.53	−0.52	0.00	−0.16	1.16
TA-C_1-a	0.06	−0.69 (−0.71)	−0.37 (−0.29)	−0.02	−0.37 (−0.51)	1.39 (1.51)
TA-C_1-b	0.06	−0.76	−0.30	−0.01	−0.49	1.50
TA-C_1-c	0.05	−0.76	−0.29	0.00	−0.53	1.54
TA-C_1-d	0.05	−0.73	−0.32	0.00	−0.48	1.48

3.4 Influences of PVP

We have discussed above the influences of PVP on the geometry, E_{ads}, charge transfer, and spin density on the molecularly or dissociatively adsorbed O_2 complexes. Here we further explore the variations in the Kohn–Sham orbitals of the neutral and

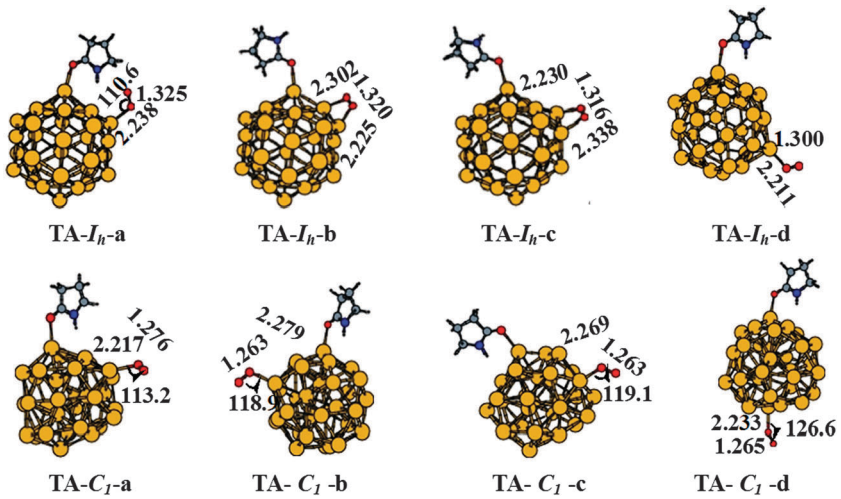

Fig. 5 TPSS/def2-QZVPP optimized structures of anionic O_2:Au_{32}(I_h):PVP and O_2:Au_{32}(C_1):PVP in which O_2 is molecularly adsorbed. The bond lengths are given in Å and the angles in degree.

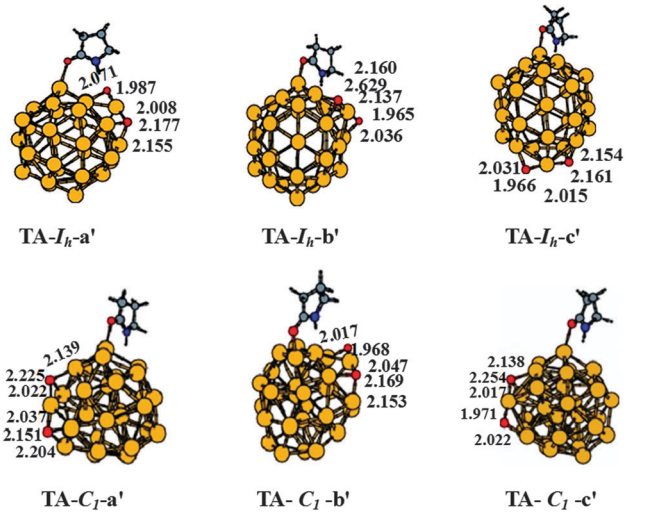

Fig. 6 TPSS/def2-QZVPP optimized structures of anionic O–$Au_{32}(I_h)$–O:PVP and O–$Au_{32}(C_1)$–O:PVP in which O_2 is dissociatively adsorbed. The bond lengths are given in Å.

Table 8 Relative energy (ΔE, in eV) and adsorption energy (E_{ads}, in eV) of anionic O–$Au_{32}(I_h)$–O:PVP and O–$Au_{32}(C_1)$–O:PVP. See Fig. 6 for the structures. In parentheses are quantities for corresponding Au_{32}:O_2 complexes without PVP

	TPSS		PBE	BLYP
	ΔE(eV)	E_{ads}(eV)	ΔE(eV)	ΔE(eV)
TA-I_h-a′	0.00	1.20 (0.81)	0.00	0.00
TA-I_h-b′	0.26	0.95	0.23	0.25
TA-I_h-c′	0.34	0.86	0.30	0.33
TA-C_1-a′	0.00	1.20 (0.76)	0.00	0.00
TA-C_1-b′	0.29	0.90	0.20	0.25
TA-C_1-c′	0.45	0.74	0.80	0.84

Table 9 Net charge (in au) and spin density (in au) of anionic O–$Au_{32}(I_h)$–O:PVP and O–$Au_{32}(C_1)$–O:PVP, see Fig. 6 for the structures. In parentheses are quantities for corresponding Au_{32}:O_2 complexes without PVP

	Net charge			Spin density		
	PVP	$Au_{32}(C_1)$	O_2	PVP	$Au_{32}(C_1)$	O_2
TA-I_h-a′	0.02	1.21 (1.21)	−2.23 (−2.21)	0.00	0.75 (0.72)	0.25 (0.28)
TA-I_h-b′	0.05	1.13	−2.18	0.00	0.67	0.33
TA-I_h-c′	0.04	1.12	−2.16	0.00	0.60	0.40
TA-C_1-a′	0.05	1.19 (1.16)	−2.24 (−2.16)	0.00	0.89 (0.89)	0.11 (0.11)
TA-C_1-b′	0.06	1.09	−2.15	0.01	0.89	0.09
TA-C_1-c′	0.06	1.03	−2.09	0.00	0.67	0.33

anionic Au_{32} and their adsorbing complexes in the presence of PVP. Since Au_{32} donates its electrons to O_2 in the O_2 activation, we focus on the variations in its HOMO orbital. Fig. 7 compares the HOMO orbitals of anionic $Au_{32}(I_h)$ and neutral $Au_{32}(C_1)$ before and after PVP adsorption. In the adsorbed systems, the HOMO orbitals are mainly contributed by the Au_{32} parts with

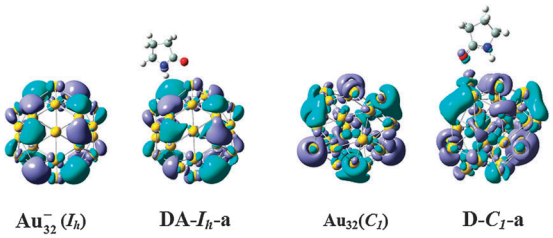

Fig. 7 HOMO orbitals of the stable Au_{32} and Au_{32}:PVP complexes.

rather small differences from those of corresponding bare clusters, indicating that the HOMO of Au_{32} basically retains its characteristics when PVP is attached. The HOMOs of neutral $Au_{32}(I_h)$ and anionic $Au_{32}(C_1)$, which are not presented, exhibit the same features. Furthermore, Fig. 8 compares the HOMOs of O_2 adsorbed Au_{32} with and without PVP. In the molecular adsorption, electrons move from Au_{32} to the anti-bond orbital of O_2 which activates the O_2 by lengthening the O–O bond. In $Au_{32}^-(I_h)$:O_2, the HOMO is mainly contributed by O_2 because of the strong electron-donating tendency of $Au_{32}^-(I_h)$. The presence of PVP leads to small changes at the region near the Au–O bond. In $Au_{32}(C_1)$:O_2 and $Au_{32}^-(C_1)$:O_2, the contributions from O_2 are not as great as in $Au_{32}^-(I_h)$:O_2, but are remarkable compared to those on the Au_{32}^- part. Again, PVP leads to rather small changes in their HOMOs. In the dissociative adsorption, the O atoms do not show more contributions to the HOMOs which distribute across the Au_{32} and the two O atoms and are not affected by the PVP attachment. In other words, PVP neither contributes to the HOMOs nor shows a remarkable difference in HOMOs in the O_2 adsorbed systems.

Quite similar band structures were noted in the projected density of states (PDOS) of the most stable O_2:$Au_{32}(C_1)$ and O_2:$Au_{32}(C_1)$:PVP complexes, as displayed in Fig. 9. Upon PVP attachment, the HOMO–LUMO gaps, the locations and compositions of occupied and virtual bands, and the distributions near the Fermi levels do not show distinct variations. Small HOMO–LUMO gaps were obtained for all these complexes. The occupied bands near the Fermi levels are composed of orbitals of s-, d- and p-characters. The s-character dominates for the complexes with molecularly adsorbed O_2, while the p-character increases for the complexes with dissociated O_2. The d-character dominates in the bands about 1.0–1.5 eV lower than the Fermi level. The dissociative adsorption of O_2 deepens the d-character bands by about 0.5 eV. The virtual bands are dominated by orbitals of s- and p-characters. Similar features were found in the PDOS of $Au_{32}(I_h)$ complexes.

It should be mentioned that three more issues important to the O_2 activation on the Au_{32} surfaces were not considered in this study. One is the kinetics of O_2 dissociation. The energy barriers of O_2 activation measure the catalytic activity of the Au_{32} clusters and could be interesting for the catalyst design. While the theme of this work is to understand how the PVP ligand affects the structural stability and electronic properties of bare and O_2 adsorbed Au_{32} clusters, and the locations of

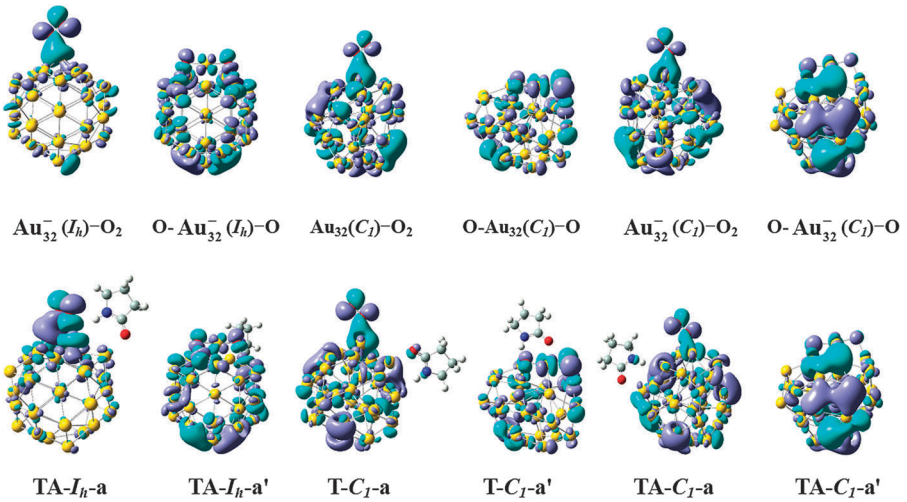

Fig. 8 HOMO orbitals of the stable Au_{32}:O_2, O–Au_{32}–O, O_2:Au_{32}:PVP and O–Au_{32}–O:PVP complexes.

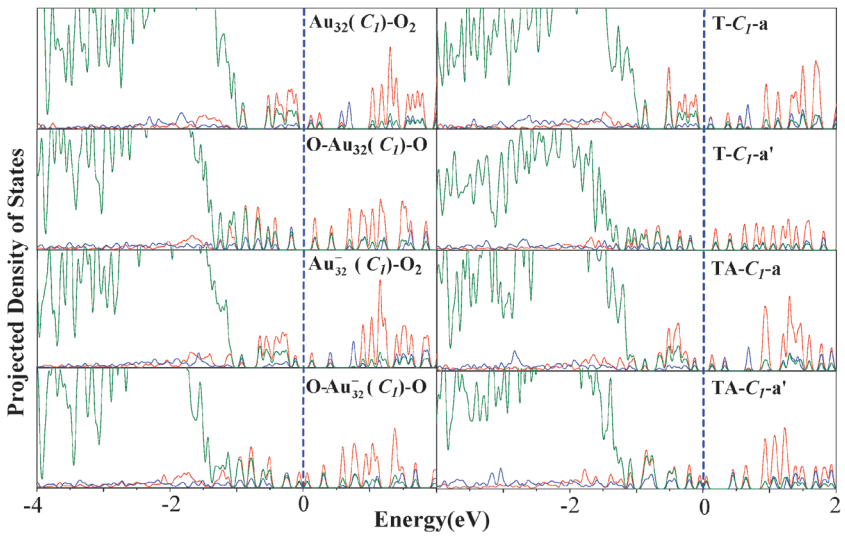

Fig. 9 Projected density of states of the most stable neutral and anionic $Au_{32}(C_1)$:O_2, O–$Au_{32}(C_1)$–O (left), and their complexes with PVP (right). The Fermi level is set at 0 eV. The s-, p-, d-type contributions are in red, blue and green respectively.

transition-state structures for the systems with 32 Au atoms and 8 more heavy atoms are computationally demanding and extremely difficult, we would leave this issue for future study. Secondly, weak interaction exists in some of the studied systems, such as PVP:Au_{32}, *etc.* Although such interaction has a rather small effect in comparison with the strong interaction between Au_{32} and O_2, dispersion correction in the functionals is suggested for a precise assessment. The last issue is the PVP coverage effect. For simplicity, only one PVP molecule was included in our computational model. As one or more PVPs adsorb on the Au_{32} surfaces, their coverage could affect the subsequent adsorption of PVP and O_2. In a DFT study,[61] the structures of Au_{13} with 1–4 PVP ligands were investigated and a decreasing E_{ads} with the PVP number was predicted. Since only weak PVP–Au_{32} interaction was noted, the structural and electronic properties of O_2 adsorbed Au_{32} clusters are hardly influenced by PVP. Our computational model is reasonable to address the interaction among O_2, Au_{32} and PVP.

4. Conclusions

DFT calculations with TPSS, PBE and BLYP functionals were performed to study the structural and electronic properties of O_2 adsorbed Au_{32} clusters under the protection of PVP. The low-lying isomers of Au_{32}:O_2, Au_{32}:PVP, and O_2:Au_{32}:PVP were identified from a large number of candidate structures which were constructed by placing O_2 and/or PVP on the surfaces of two widely studied Au_{32} isomers, I_h and C_1, in their neutral or anionic forms. The three functionals produce similar energy orders for the isomers. In the presence of PVP, the dissociative O_2 adsorption is more favorable than the corresponding molecular adsorption on neutral $Au_{32}(C_1)$, while both patterns are

favored on neutral $Au_{32}(I_h)$. For the anionic $Au_{32}(I_h)$ and $Au_{32}(C_1)$, the dissociative adsorptions have systematically larger E_{ads} values than the corresponding molecular adsorptions.

The influence of PVP was studied by comparing the geometrical and electronic structures of Au_{32}:O_2 complexes with and without PVP pre-adsorption. Firstly, PVP adsorbs weakly on the cluster surface. This is a typical physisorption with few changes in PVP and Au_{32} structures. Secondly, only very small changes in geometry, adsorption energy, charge redistribution, spin density, and density of states were noted for Au_{32}:O_2 complexes in the pre-adsorption of PVP. The O_2 activation on Au_{32} is hardly affected by the PVP. Thirdly, the weak electron-donating ability of PVP favors to some extent the Au_{32} activity towards O_2 *via* a cooperative adsorption of PVP and O_2. All of the above arguments constitute the structural basis of PVP as the protective ligand for Au clusters.

Acknowledgements

SY thanks the Fundamental Research Funds (No.11NZYBS07) for the Central Universities, Southwest University for Nationalities. MY thanks the financial support from NSFC (No. 20873088) and Open Funds of State Key Laboratory of Physical Chemistry of Solid Surfaces (Xiamen University, No. 201109)

References

1 M. Haruta, *Catal. Today*, 1997, **36**, 153–166.
2 M. Valden, X. Lai and D. W. Goodman, *Science*, 1998, **281**, 1647–1650.
3 T. S. Kim, J. D. Stiehl, C. T. Reeves, R. J. Meyer and C. B. Mullins, *J. Am. Chem. Soc.*, 2003, **125**, 2018–2019.
4 C. Lemire, R. Meyer, S. Shaikhutdinov and H. J. Freund, *Angew. Chem., Int. Ed.*, 2004, **43**, 118–121.
5 A. Sanchez, S. Abbet, U. Heiz, W. D. Schneider, H. Hakkinen, R. N. Barnett and U. Landman, *J. Phys. Chem. A*, 1999, **103**, 9573–9578.
6 J. Guzman and B. C. Gates, *J. Am. Chem. Soc.*, 2004, **126**, 2672–2673.
7 N. Lopez, T. V. W. Janssens, B. S. Clausen, Y. Xu, M. Mavrikakis, T. Bligaard and J. K. Norskov, *J. Catal.*, 2004, **223**, 232–235.
8 A. A. Herzing, C. J. Kiely, A. F. Carley, P. Landon and G. J. Hutchings, *Science*, 2008, **321**, 1331–1335.
9 A. Lyalin and T. Taketsugu, *J. Phys. Chem. C*, 2009, **113**, 12930–12934.
10 A. Franceschetti, S. J. Pennycook and S. T. Pantelides, *Chem. Phys. Lett.*, 2003, **374**, 471–475.
11 B. Yoon, H. Häkkinen and U. Landman, *J. Phys. Chem. A*, 2003, **107**, 4066–4071.
12 H. J. Zhai and L. S. Wang, *J. Chem. Phys.*, 2005, **122**, 051101.
13 Y. Wang and X. G. Gong, *J. Chem. Phys.*, 2006, **125**, 124703.
14 D. W. Yuan and Z. Zheng, *J. Chem. Phys.*, 2004, **120**, 6574–6584.
15 G. Mills, M. S. Gordon and H. Metiu, *J. Chem. Phys.*, 2003, **118**, 4198–4205.
16 H. C. Liu, A. I. Kozlov, A. P. Kozlova, T. Shido and Y. Iwasawa, *Phys. Chem. Chem. Phys.*, 1999, **1**, 2851–2860.
17 W. Huangab and L. S. Wang, *Phys. Chem. Chem. Phys.*, 2009, **11**, 2663–2667.
18 T. Y. Wang, B. H. Li, J. H. Yang, H. Chen and L. Chen, *Phys. Chem. Chem. Phys.*, 2011, **13**, 7112–7120.
19 P. Frondelius, H. Häkkinenb and K. Honkalac, *Phys. Chem. Chem. Phys.*, 2010, **12**, 1483–1492.
20 A. Roldán, J. M. Ricart, F. Illas and G. Pacchioni, *Phys. Chem. Chem. Phys.*, 2010, **12**, 10723–10729.
21 L. Prati and M. Rossi, *J. Catal.*, 1998, **176**, 552–560.
22 S. Carrettin, P. McMorn, P. Johnston, K. Griffin and G. J. Hutchings, *Chem. Commun.*, 2002, 696–697.
23 M. D. Hughes, Y. J. Xu, P. Jenkins, P. McMorn, P. Landon, D. I. Enache, A. F. Carley, G. A. Attard, J. Hutchings, F. King, E. H. Stitt, P. Johnston, K. Griffin and C. J. Kiely, *Nature*, 2005, **437**, 1132–1135.
24 A. Abad, P. Concepción, A. Corma and H. García, *Angew. Chem., Int. Ed.*, 2005, **44**, 4066–4069.
25 T. Hayashi, K. Tanaka and M. Haruta, *J. Catal.*, 1998, **178**, 566–575.
26 M. Walter, M. Moseler, R. L. Whetten and H. Häkkinen, *Chem. Sci.*, 2011, **2**, 1583–1587.
27 Y. Negishi, K. Nobusada and T. Tsukuda, *J. Am. Chem. Soc.*, 2005, **127**, 5261–5270.
28 Y. Negishi, W. Kurashige and U. Kamimura, *Langmuir*, 2011, **27**, 12289–12292.
29 H. Tsunoyama and T. Tsukuda, *J. Am. Chem. Soc.*, 2009, **131**, 18216–18217.
30 P. Maity, H. Tsunoyama, M. Yamauchi, S. Xie and T. Tsukuda, *J. Am. Chem. Soc.*, 2011, **133**, 20123–20125.
31 H. Tsunoyama, N. Ichikuni, H. Sakurai and T. Tsukuda, *J. Am. Chem. Soc.*, 2009, **131**, 7086–7093.
32 H. Tsunoyama, H. Sakurai and T. Tsukuda, *J. Am. Chem. Soc.*, 2005, **127**, 9374–9375.
33 H. Tsunoyama, H. Sakurai and T. Tsukuda, *Chem. Phys. Lett.*, 2006, **429**, 528–532.
34 I. L. Garzón, C. Rovira, K. Michaelian, M. R. Beltran, P. Ordejorn, J. Junquera, D. Sanchez-Portal, E. Artacho and J. M. Soler, *Phys. Rev. Lett.*, 2000, **85**, 5250–5251.
35 H. Häkkinen, M. Walter and H. Grönbeck, *J. Phys. Chem. B*, 2006, **110**, 9927–9931.
36 D. Jiang, W. Chen, R. L. Whetten and Z. Chen, *J. Phys. Chem. C*, 2009, **113**, 16983–16987.
37 T. Iwasa and K. Nobusada, *J. Phys. Chem. C*, 2007, **111**, 45–49.
38 J. Akola, M. Walter, R. L. Whetten, H. Hakkinen and H. Grönbeck, *J. Am. Chem. Soc.*, 2008, **130**, 3756–3757.
39 Y. Pei, Y. Gao and X. C. Zeng, *J. Am. Chem. Soc.*, 2008, **130**, 7830–7832.
40 D. Jiang, M. L. Tiago, W. D. Luo and S. Dai, *J. Am. Chem. Soc.*, 2008, **130**, 2777–2779.
41 D. Jiang, W. Luo, M. L. Tiago and S. Dai, *J. Phys. Chem. C*, 2008, **112**, 13905–13910.
42 Y. Gao, N. Shao and X. C. Zeng, *ACS Nano*, 2008, **2**, 1497–1503.

43 Y. K. Han, H. Kim, J. Jung and Y. C. Choi, *J. Phys. Chem. C*, 2010, **114**, 7548–7552.
44 T. Li, G. Galli and F. Gygi, *ACS Nano*, 2008, **2**, 1896–1902.
45 O. Lopez-Acevedo, J. Akola, R. L. Whetten, H. Grönbeck and H. Häkkinen, *J. Phys. Chem. C*, 2009, **113**, 5035–5038.
46 X. Gu, M. Ji, S. H. Wei and X. G. Gong, *Phys. Rev. B: Condens. Matter Mater. Phys.*, 2004, **70**, 205401.
47 A. F. Jalbout, F. F. Contreras-Torres, L. A. Pérez and I. L. Garzón, *J. Phys. Chem. A*, 2008, **112**, 353–357.
48 M. P. Johansson, A. Lechtken, D. Schooss and M. M. Kappes, *Phys. Rev. A*, 2008, **77**, 053202.
49 F. Weigend, F. Furche and R. Ahlrichs, *J. Chem. Phys.*, 2003, **119**, 12753–12762.
50 J. H. Wood and A. M. Boring, *Phys. Rev. B: Condens. Matter Mater. Phys.*, 1978, **18**, 2701–2711.
51 *TURBOMOLE V5-9-1*, University of Karlsruhe, 2007.
52 K. P. Huber and G. Herzberg, *Molecular Spectra and Molecular Structure*, Van Nostrand Reinhold, New York, 1979.
53 G. Mills, M. S. Gordon and H. Metiu, *Chem. Phys. Lett.*, 2002, **359**, 493–499.
54 K. Eichkorn, O. Treutler, H. Oehm, M. Haeser and R. Ahlrichs, *Chem. Phys. Lett.*, 1995, **242**, 652–660.
55 M. Sierka, A. Hogekamp and R. Ahlrichs, *J. Chem. Phys.*, 2003, **118**, 9136–9148.
56 J. P. Perdew, K. Burke and M. Ernzerhof, *Phys. Rev. Lett.*, 1996, **77**, 3865–3868.
57 A. D. Becke, *Phys. Rev. A: At., Mol., Opt. Phys.*, 1988, **38**, 3098–3100.
58 C. L. Lee, W. Yang and R. G. Parr, *Phys. Rev. B: Condens. Matter Mater. Phys.*, 1988, **37**, 785–789.
59 J. Tao, J. P. Perdew, V. N. Staroverov and G. E. Scuseria, *Phys. Rev. Lett.*, 2003, **91**, 46401.
60 A. E. Reed, L. A. Curtiss and F. Weinhold, *Chem. Rev.*, 1988, **88**, 899–926.
61 M. Okumura, Y. Kitagawa, T. Kawakami and M. Haruta, *Chem. Phys. Lett.*, 2008, **459**, 133–136.